Featured in Physics

Realization of efficient tuning of the Fermi level in iron-based ferrimagnetic alloys

N. Yamashita,[1,*] E. Shigematsu,[1] S. Honda,[2] R. Ohshima,[1] M. Shiraishi,[1] and Y. Ando[1,3,†]

[1]*Department of Electronic Science and Engineering, Kyoto University, Kyoto, Kyoto, 615–8510, Japan*

[2]*Department of Pure and Applied Physics, Kansai University, Suita, Osaka, 564–8680, Japan*

[3]*PRESTO, Japan Science and Technology Agency, Honcho, Kawaguchi, Saitama 332–0012, Japan*

(Received 8 October 2021; accepted 8 September 2022; published 12 October 2022)

The Stoner criterion allows only three single elements possessing room-temperature (RT) ferromagnetism: cobalt (Co), nickel (Ni), and iron (Fe). Although these three elements have played central roles in magnetism-based materials, their large work function (4.5 $\sim$ 5.2 eV) is becoming a non-negligible obstacle for realization of spin devices using nonmetallic materials with finite energy gaps, because injection of electron spins into these nonmetallic materials is strongly hampered due to the large Schottky barrier height. Hence, a novel ferromagnetic or ferrimagnetic material simultaneously possessing RT ferromagnetism or ferrimagnetism and high Fermi energy is strongly required. Here, we show that an Fe-based alloy, iron-gadolinium (FeGd), allows circumvention of the obstacle. Surprisingly, only 20% of Gd incorporation in Fe dramatically modulates the Fermi energy from -4.8 to -3.0 eV, which is the largest modulation in all metallic alloys reported thus far. The coexistence of ferrimagnetism and nonzero spin polarization at RT of FeGd supports its abundant potential for future applications in low-carrier-density materials such as monolayer, organic, and nondegenerate inorganic semiconductors.

DOI: 10.1103/PhysRevMaterials.6.104405

I. INTRODUCTION

The number of elements exhibiting room-temperature (RT) ferromagnetism is strongly restricted by the Stoner criterion [1]. Only iron (Fe), cobalt (Co), and nickel (Ni) exhibit Curie temperatures (T_c) much higher than RT and a sizeable spin polarization at the Fermi level (E_F) among single elements. This restriction has encouraged scientists to synthesize a wide variety of compound ferromagnets and ferrimagnets by using any of them as a host material. The other restriction for single-element ferromagnets is that the E_F of these three ferromagnetic elements is far below the vacuum level (-4.5 to -5.2 eV) [2], mainly because $3d$ electrons are responsible for ferromagnetism. This strong restriction invokes difficulty in selecting suitable ferromagnetic and ferrimagnetic materials, especially for the formation of heterojunctions without unwanted barriers and depletion regions for nonmetallic materials, because the majority of ferromagnetic and ferrimagnetic materials are Fe/Co/Ni-based specimens and their E_F is far below the vacuum level. Indeed, the difficulty becomes quite salient in spin-polarized carrier injection (extraction) into (from) low-carrier-density materials such as organic semiconductors, atomically flat semiconductors such as transition metal dichalcogenides (TMDs) [3], Weyl semimetals, and so forth, although they are now playing central roles in modern condensed matter physics. One good example of the difficulty is a ferromagnetic material–semiconductor (inorganics, organics, and TMDs) interface [4]. Since most ferromagnetic materials possess a low E_F, i.e., high work function (WF), the injection of negatively charged spin carriers (electrons) into materials with a low carrier density is difficult. Although a limited approach to circumvent this obstacle is to dope electrons to the host semiconducting materials, this approach does not allow versatile control of the polarity of spin carriers, and the dense dopant strongly suppresses the lifetime of injected spins into semiconducting materials in principle by the Elliott-Yafet mechanism [5]. Thus, carrier doping makes the whole device system more intricate and/or hampers the creation of ambipolar magnetic/spintronic devices and logic systems, such as spin lasers [6], spin light-emitting diodes [7], spin transistors [8], and spin logics [9]. Notably, this problem has not manifested itself in ferromagnetic/nonmagnetic–metal heterojunctions because no Schottky barrier or depletion region forms at the heterointerface, and thus, this difficulty arises in the modern condensed matter physics era. Given the current status of materials science, a material possessing simultaneous ferromagnetism or ferrimagnetism and high E_F (low WF) is urgently needed to circumvent these obstacles. Here, we report drastic WF modulation of iron-gadolinium (Gd) binary alloys, $Fe_{100-x}Gd_x$, since pure Gd has a low WF. $Fe_{78}Gd_{22}$ possesses an extraordinarily low WF and exhibits the coexistence of RT ferrimagnetism and nonzero spin polarization at E_F, which fulfils the conditions for bypassing the previously mentioned obstacles to accelerate physical and materials science. Surprisingly, only a 20% Gd incorporation in Fe enables the dramatic modulation of WF from 4.9 to 3.0 eV—the most efficient modulation among all metallic alloys, while the T_c is still higher than RT.

*Present address: Faculty of Information Science and Electrical Engineering, Kyushu University, Fukuoka, Fukuoka, 819–0395, Japan.

†ando.yuichiro.5s@kyoto-u.ac.jp

II. SAMPLE FABRICATION AND EXPERIMENTAL PROCEDURE

$Fe_{100-x}Gd_x$ thin films were deposited in an ultra-high vacuum chamber (base pressure $< 1 \times 10^{-7}$ Pa). Fe was evaporated by resistive heating, and Gd was evaporated by electron-beam heating. To control the composition of x, the deposition rate of each metal was monitored by a quartz crystal thickness monitor. A thermally oxidized Si substrate was employed for the measurements of the magnetization curves and the anomalous Hall effect (AHE) signals. Hall bar-shaped $Fe_{100-x}Gd_x$ channels for measurement of the AHE were fabricated by electron beam lithography and a liftoff process. For fabrication of the devices for I - V measurements, n-type Si with moderate doping (10^{15} cm^{-3} of phosphorous was doped) was employed. The 1-cm × 1-cm Si substrates were cleaned using SEMICO-CLEAN23, ultrasonicated, and then dipped into 2% aqueous HF solution. On the back of the substrate, an ohmic $Au_{98}Sb_2$/n-Si contact was formed using thermal evaporation in an ultra-high vacuum chamber followed by thermal annealing at 350 °C. After forming the backside ohmic contact, the top $Fe_{100-x}Gd_x$ electrodes were fabricated by a liftoff process. Before deposition of the $Fe_{100-x}Gd_x$ layer, the naturally oxidized layer was removed by dipping the substrates for 30 seconds into 2% HF solution less than 5 minutes before being put into the vacuum chamber. Two different $Fe_{100-x}Gd_x$ layers were fabricated to measure the WF. One has a uniform Gd composition (single-composition sample), and the other has an intentionally modulated Gd composition along the surface normal (gradated-composition sample). For the fabrication of the gradated-composition sample, Gd was first deposited. After the deposition of a 10 -nm-thick Gd layer, the shutter for Fe deposition was opened, and then the deposition rate of Gd was gradually decreased from 2.0 nm/min down to 0 nm/min. The deposition rate of Fe was kept at 1.0 nm/min. Finally, a 20-nm-in-thick Fe layer was formed. The crystal structure of the $Fe_{100-x}Gd_x$ layer was amorphous except for the pure Fe ($x = 0$) or Gd ($x = 100$) layers, which were polycrystalline (see Supplemental Material (SM)-1 [10]).

UV photoelectron spectroscopy (UPS) equipped with x-ray photoelectron spectroscopy (XPS) (Versa Probe, ULVAC-PHI) was used for the measurements of the WF. The surface of the measured samples was milled by Ar^+ ion milling, and the WF and x were measured by UPS and XPS, respectively. To measure the UPS spectra, the samples were irradiated with UV light with a photon energy of 21.22 eV, and a bias voltage of −10 V was applied. For the XPS measurements, the samples were irradiated with x-rays with a photon energy of 1486.6 eV.

The magnetization curves were measured by using a vibrating sample magnetometer with a temperature-controlling system (VSM-5, Toei Industry). The AHE measurements were carried out using a physical property measurement system (PPMS, Quantum Design). A constant charge current of 0.1 mA was applied, and the dc voltage was monitored under the application of a perpendicular magnetic field.

III. WF OF $Fe_{100-x}Gd_x$ ALLOYS

The WF of $Fe_{100-x}Gd_x$ alloys with various values of x was measured using UPS equipped with XPS. The atomic composition was simultaneously measured by XPS, which enables a direct comparison of x and WF at the same surface. The UPS spectra at various values of x, are summarized in Fig. 1(a). The secondary edge of the UPS spectrum corresponding to the photoelectrons with the lowest energy was adjusted to −21.22 eV (see SM-2 [10,11]). The positions of the E_F were determined by fitting the convolution of the Fermi–Dirac function to a Gaussian function [11], as indicated by the red dashed lines. The WF of pure Fe ($x = 0$) and Gd ($x = 100$) was 4.9 ± 0.1 and 2.9 ± 0.1 eV, respectively, comparable to a previous study [2]. The peaks in the UPS spectra of pure Fe ($x = 0$) and pure Gd ($x = 100$) located at approximately 0.8 (indicated by the blue arrow) and 5.0 eV (indicated by the red arrow) below E_F correspond to the high density of state of the majority spins of the 3d electron in bcc-Fe and those of the 4f electrons of hcp-Gd, respectively, which is supported by first-principles calculations carried out using the Vienna *Ab initio* Simulation Package (VASP) (see SM-3 [10,12–14]). The central result of this study is that the WF shifts drastically toward a lower value from 4.9 ± 0.1 eV to 3.1 ± 0.1 eV when x changes from 0 to 20. The WF at $x = 20$ is comparable to that of pure Gd, even though the composition of Gd is just 20%. Surprisingly, the peak of the 3d electron for the $Fe_{100-x}Gd_x$ alloy (indicated by the blue arrow) shifts toward higher energy when x increases from 0 to 20, indicating that the 3d electrons, main contributors of ferromagnetism and spin polarization, still contribute to the conductance even for the noticeable change in E_F. It is noted that because the crystal structure of $Fe_{100-x}Gd_x$ alloys are amorphous except for the pure Fe ($x = 0$) and Gd ($x = 100$) samples, a calculated band structure of a crystalline $Fe_{100-x}Gd_x$ by using VASP is not comparable to the experimental results. A simple superposition of the band structures of Fe and Gd is also incorrect. However, since the peak feature indicated by the blue arrow is gradually shifted from 3d electrons of Fe with increasing x, as shown in Fig. 1(a), we concluded that these peaks are related to 3d electrons of Fe.

The x-dependence of the WF is summarized in Fig. 1(b). WF was drastically reduced down to 3.1 ± 0.1 eV when x was increased from 0 to 20, and showed almost constant value for $x > 20$. Similar results were also obtained for the single-composition samples, as shown in Fig. 1(b). The notable change in WF has not been observed in other ferromagnetic alloys, such as $Co_{100-x}Fe_x$ [15] and $Ni_{100-x}Fe_x$ [16]. We stress that the large modulation of the WF is also notable among nonmagnetic alloys. Figure 1(c) shows a summary of the modulation efficiency of the WF, η, for a variety of binary alloys. η was obtained from the change in the WF achieved by adding a low WF element of 1% (in the case of $Fe_{100-x}Gd_x$ alloys, Gd corresponds to the "low WF element"). Because the data (except for those of the $Fe_{100-x}Gd_x$ alloys) were quoted from previous works [17–22], the number of points varies among the works. Therefore, the averaged η was calculated by using at least three points whose x range was approximately 20% to avoid overestimation or underestimation. For $Fe_{100-x}Gd_x$, η is 88.4 meV/%—more than 10-fold that in ferromagnetic metals consisting of 3d transition elements ($Co_{100-x}Fe_x$ and $Ni_{100-x}Fe_x$), and the highest value among binary alloys that include nonmagnetic materials.

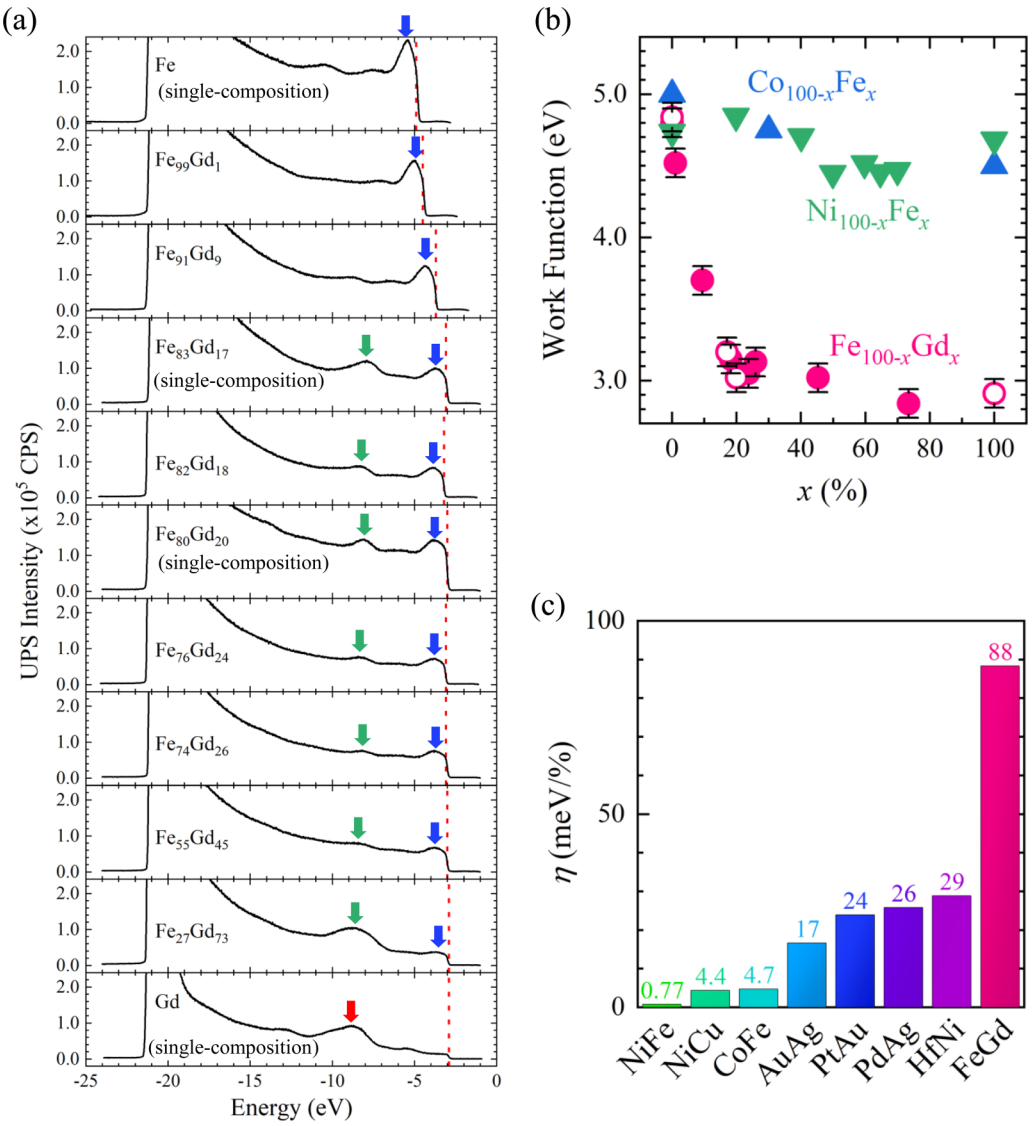

FIG. 1. (a) Results of the UPS measurements. The x-axis represents the energy of the electron on the basis of the vacuum level, and the y-axis shows the intensity in units of counts per second (CPS). The UPS spectra of $Fe_{100}Gd_0$, $Fe_{83}Gd_{17}$, $Fe_{80}Gd_{20}$, and Fe_0Gd_{100} samples were obtained from the single-composition samples, whereas the other spectra were obtained sequentially from the gradated-composition sample. The red dashed lines represent the Fermi energy estimated by fitting using convolution of the Fermi–Dirac function and the Gaussian function. The blue arrows indicate the UPS peaks that are identical to the energy of the Fe 3d band. The green and red arrows indicate the UPS peaks that are identical to the energy of the Gd 4f band. (b) Comparison of the composition dependence of the WF among ferromagnetic/ferrimagnetic alloys. The x-axis shows the surface composition, and the y-axis shows the measured WFs. The green and blue plots represent the WF values of $Ni_{100-x}Fe_x$ and $Co_{100-x}Fe_x$. The pink plots represent the WF values of $Fe_{100-x}Gd_x$. The filled (open) circles represent the results of the gradated (single)-composition sample. (c) Comparison of the WF modulation efficiency η based on the composition of binary alloys for a variety of alloys. η is the change in the WF due to adding a low WF element of 1%.

IV. MAGNETIZATION CURVES AND ANOMALOUS HALL MEASUREMENTS

Materials involving finite magnetization at RT and such a large E_F variation are useful for spintronic and spin-orbitronic applications that require a specific E_F. Therefore, we carried out magnetization measurements by using a vibrating sample magnetometer at 300 K. The atomic composition was measured by XPS. The measured magnetization curves (M–B_x curves) of the single-composition $Fe_{100-x}Gd_x$ samples are shown in Fig. 2(a)–2(d). An external magnetic field with a magnetic flux density of B_x was applied along the in-plane direction of the film plane. The $Fe_{100-x}Gd_x$ samples with $x = 21$, 14, and 0 exhibited saturation of the magnetization M, indicating ferromagnetism or ferrimagnetism at 300 K [Fig. 2(b), 2(c), and 2(d), respectively]. The similar saturation in M was also obtained for the $Fe_{100-x}Gd_x$ samples with $x = 23$. In contrast, the Gd sample ($x = 100$) exhibited no saturation or hysteresis, indicating paramagnetic features due to its T_c being lower than 300 K [Fig. 2(a)]. The saturation magnetization M_s as a function of x is shown in Fig. 2(e). The reduction in M_s with increasing x for $x < 21$ is not due to a weakened exchange coupling between spins, but due to the ferrimagnetic character, i.e., magnetic compensation between

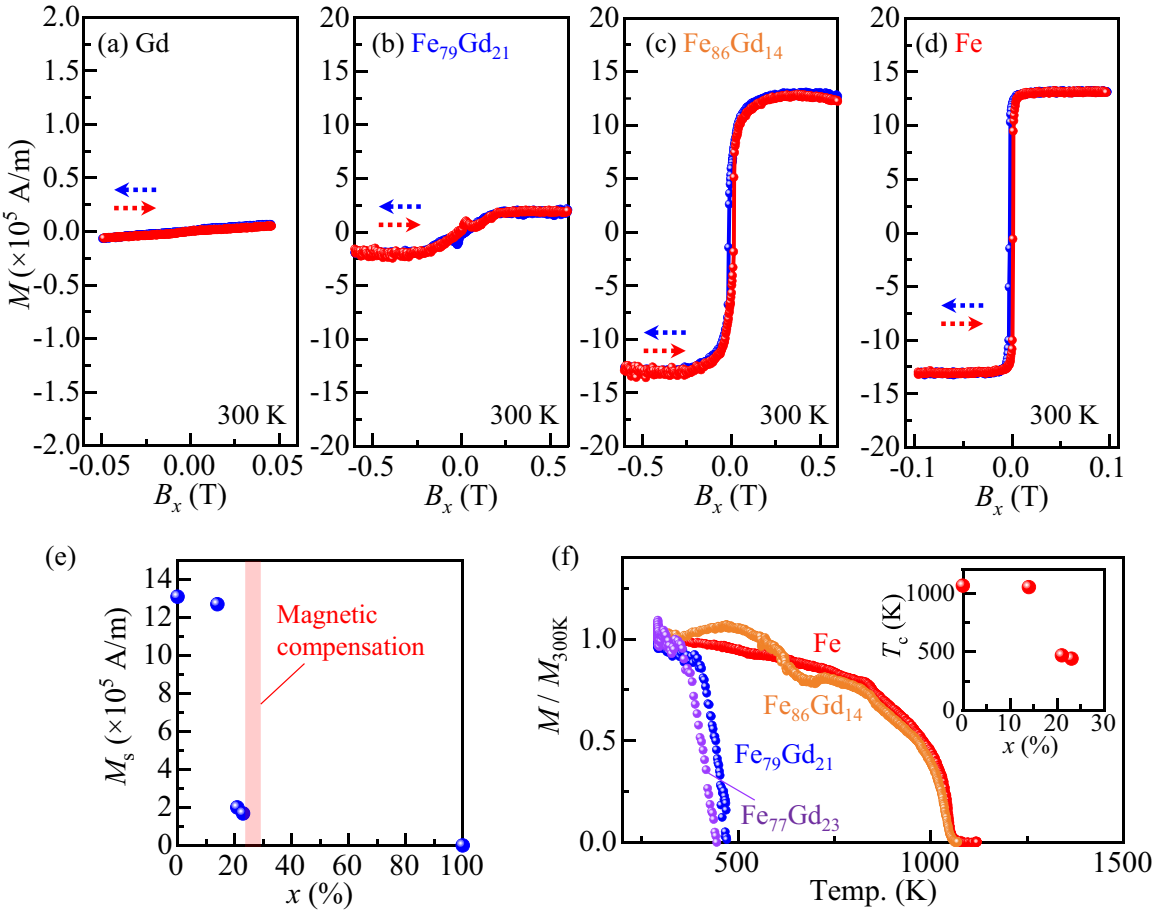

FIG. 2. Magnetization curves of $Fe_{100-x}Gd_x$ films measured at RT by using a vibrating sample magnetometer for (a) Gd, (b) $Fe_{79}Gd_{21}$, (c) $Fe_{86}Gd_{14}$, and (d) Fe single-composition samples. An in-plane magnetic field was applied to the sample. (e) Saturation magnetization M_s obtained by magnetization curves as a function of x. The pink area is the magnetic compensation area reported in Refs. [39,40]. (f) Temperature evolution of magnetization, M at $B_x = 1$ T normalized by M at 300 K for $Fe_{100-x}Gd_x$ single-composition samples. The inset shows the Curie temperature T_c as a function of x.

the Fe and Gd atoms [23]. Temperature dependence of M normalized by magnetization at 300 K, $M_{300\,K}$, under application of $B_x = 1$ T is summarized in Fig. 2(f). T_c as a function of x is summarized in the inset of Fig. 2(f). T_c of the Fe sample is roughly estimated to be 1060 K, consistent with the literature [24]. For $Fe_{86}Gd_{14}$, surprisingly, comparable T_c with that of Fe was obtained. Whereas T_c was steeply decreased for $x > 14$, T_c of $Fe_{79}Gd_{21}$ and $Fe_{77}Gd_{23}$ is sufficiently higher than 300K, indicating ferrimagnetism is sufficiently maintained even at 300 K.

The AHE was measured at various temperatures to confirm finite spin polarization at E_F. We fabricated Hall bars, as schematically shown in the inset of Fig. 3(a). We first measured the temperature dependence of resistivity ρ_{xx} of the $Fe_{100-x}Gd_x$ layers with the Hall bar structure. The results are summarized in Fig. 3(b) and 3(c). For Fe and Gd samples, ρ_{xx} was decreased with decreasing temperature and slightly saturated at low temperature, which is a typical feature of pure metals. A slightly higher ρ_{xx} of Gd than that of Fe is also consistent with previous research. In contrast, for the other $Fe_{100-x}Gd_x$ samples, ρ_{xx} was increased with decreasing temperature, a typical feature of highly disordered metals [25].

For the AHE measurements, a charge current I was applied in the x direction, and the voltage difference along the y direction (V_{xy}) was measured by sweeping the magnetic field along the z direction (B_z). The typical AHE signals, i.e., Hall resistivity, ρ_{xy}, as a function of B_z, for the $Fe_{100-x}Gd_x$ samples measured at various temperatures are plotted in Fig. 4(a)–4(d). For the Fe sample, positive ρ_{xy} was obtained for $B_z > 0$ and was saturated around 2 T. Clear AHE signals were obtained at a wide range of temperatures, from 4 to 300 K. Whereas clear AHE signals with opposite polarity to that of the Fe sample were obtained below 250 K for the Gd sample, the AHE signal almost disappeared at 300 K, indicating that spin polarization and ferromagnetism almost disappeared at 300 K, consistent with the magnetization curve shown in Fig. 2(a). It is noted that clear AHE signals were obtained even at 300 K for $Fe_{77}Gd_{23}$ and $Fe_{79}Gd_{21}$, which manifests a finite spin polarization at 300 K. The amorphous structure in the $Fe_{100-x}Gd_x (0 < x < 100)$ alloys excludes the intrinsic AHE induced by the Berry curvature; the possible origin of the AHE is the extrinsic effects, including skew scattering and side jump–spin-dependent scattering [26], and thus, we attributed the AHE to finite spin polarization at 300 K.

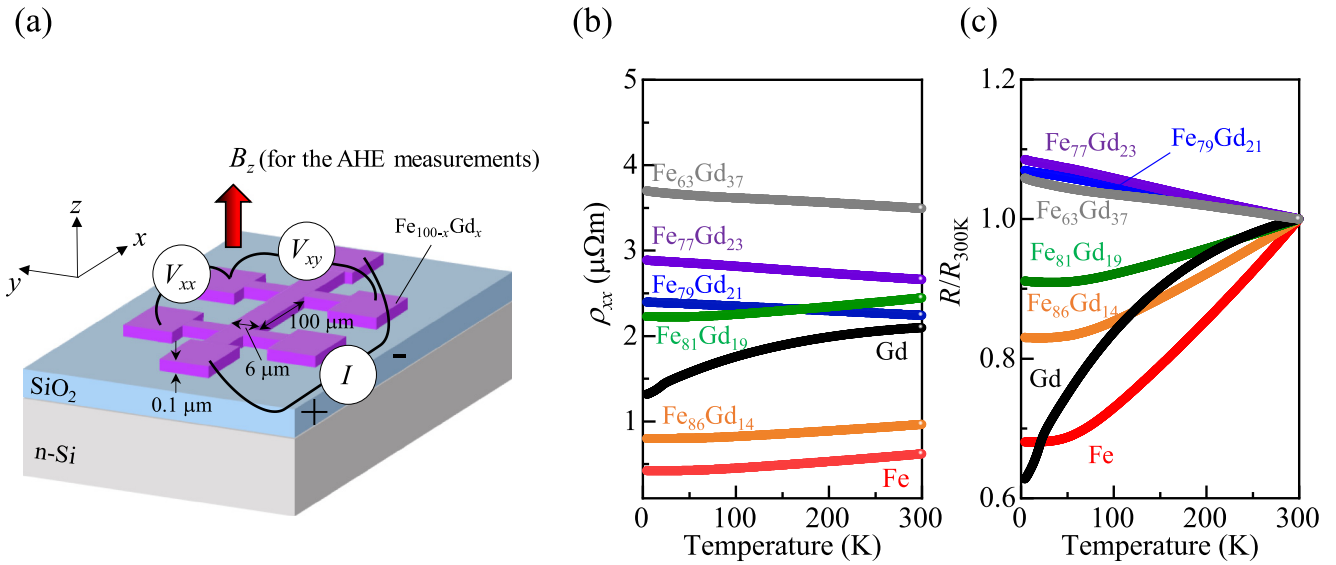

FIG. 3. (a) A schematic of the device structure for the measurements of resistivity and anomalous Hall effect. (b) Temperature dependences of resistivity ρ_{xx}, for $Fe_{100-x}Gd_x$ single-composition samples with various x. (c) Temperature dependences of ρ_{xx} normalized by ρ_{xx} at 300 K.

V. ELECTRICAL CHARACTERISTICS OF THE $Fe_{100-x}Gd_x$/n-Si INTERFACE

To confirm the highly effective modulation of the E_F at the metal–semiconductor interfaces, Schottky barrier diodes made of $Fe_{100-x}Gd_x$/n-type Si were investigated at 300 K. Vertical Schottky barrier diodes of $Fe_{100-x}Gd_x$ on the n-Si substrate were fabricated, as shown in the inset of Fig. 5(a). Capacitance–voltage measurements of the Fe–Si Schottky barrier diodes reveal a Schottky barrier height of 0.61 eV, consistent with the value in the literature [27] (see SM-4 [4,10,28,29]). The current–voltage characteristics of the Schottky barrier diodes measured at RT are shown in Fig. 5(a)–5(d). A current-rectifying characteristic was obtained in Fe/Si [Fig. 5(d)], where the ratio of on current to off current (on/off ratio) at ±1.0 V is 890. In contrast, an on/off ratio of 1 was realized for $x \geqslant 21$, indicating ohmic contacts to n-Si. Since Si is a typical semiconductor of the Bardeen limit with a considerably low S factor ($S \simeq 0.1$) [30], where S is defined as $S = \partial\Phi_B/\partial\chi_m$, and Φ_B and χ_m are the Schottky barrier height and the metal electronegativity, respectively, the E_F of the metal hardly controls the Schottky barrier height due to Fermi level pinning. The ohmic behavior of $Fe_{100-x}Gd_x$/Si($x > 21$) indicates that the WF of $Fe_{100-x}Gd_x$($x > 21$) is sufficiently lower than the electron affinity of Si (4.0 eV), which is consistent with the results of the UPS measurements shown in Fig. 1(a). For semiconductors with a Schottky limit ($S \simeq 1$), such as few-layer graphene and $SnSe_2$ [31], a sufficient modulation of the Schottky barrier height is expected by adding only a few percent Gd. For the

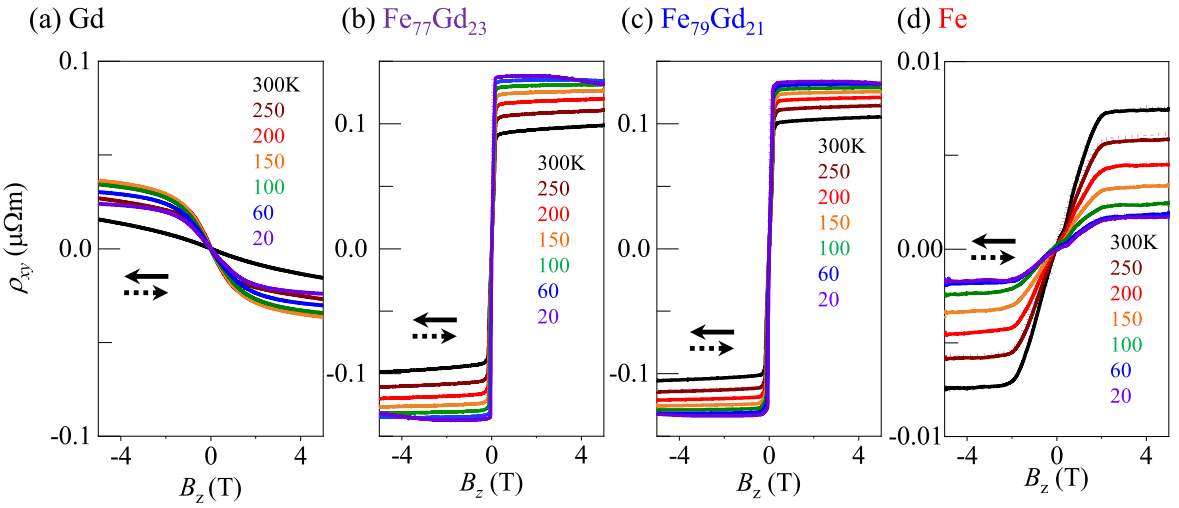

FIG. 4. [(a)–(d)] Results of anomalous Hall measurements of the Hall bar-shaped $Fe_{100-x}Gd_x$ single-composition samples at various temperatures. The Hall voltage was measured under the application of an out-of-plane magnetic field. A dc charge current of 0.1 mA was applied. The device geometry and current–voltage configuration are shown in Fig. 3(a).

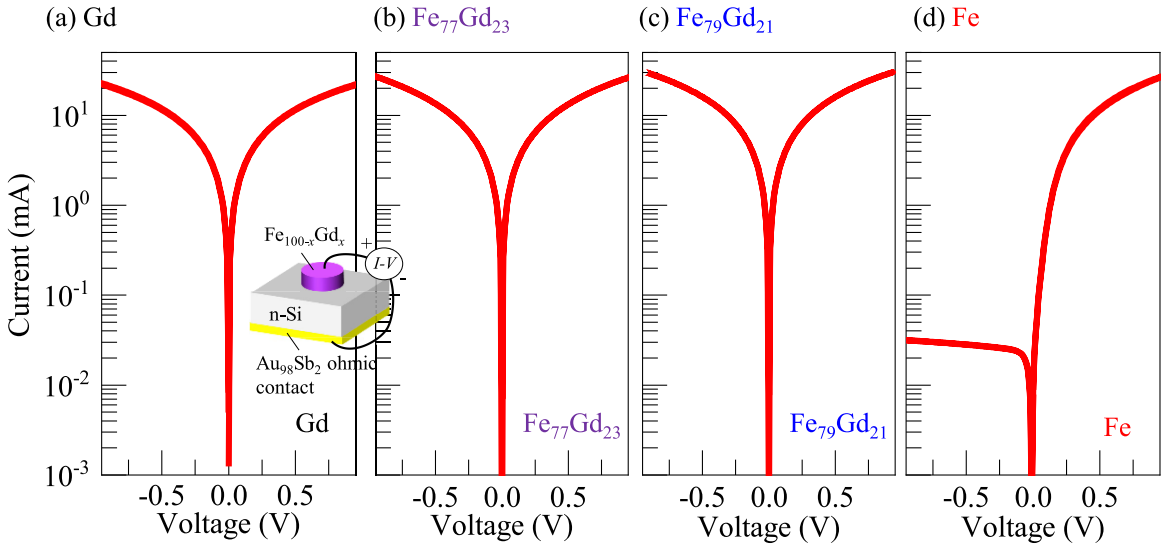

FIG. 5. [(a)–(d)] Semi-log plots of the current-rectifying characteristics for the $Fe_{100-x}Gd_x$ single-composition samples measured at 300 K. A gold (Au) antimony (Sb) ohmic contact was fabricated at the backside of the *n*-Si substrate. The device structure is shown in the inset of (a). The size of the $Fe_{100-x}Gd_x$ electrodes was 0.29 mm^2.

Si-based spintronic devices, realization of a spin injector and detector with significantly low interfacial resistance is expected by using $Fe_{100-x}Gd_x$ alloys, which is a great advantage compared to other ferromagnetic or ferrimagnetic contacts with appreciable interfacial resistance due to the existence of the Schottky barrier or oxide tunneling barrier [32,33] (see SM-6 [10,34–37]).

VI. CONCLUSION

Prior to this study, it was thought that ferromagnetic and ferrimagnetic materials restricted by the Stoner criterion have low E_F and that Schottky barriers inevitably arise at the interfaces with materials with finite energy gaps, including monolayer, organic, and nondegenerate inorganic semiconductors. We found significant modulation of the E_F in ferrimagnetic metals with a finite spin polarization at RT, which overcomes the issue of the Schottky barrier for materials with finite energy gaps. Thus, this study pioneers an approach to creating ambipolar spin devices based on these gapped materials, such as a spin laser [6], a spin light-emitting diode [38], and a spin logic gate [9], by simultaneously achieving considerably low interfacial resistance and finite spin polarization at the E_F. One of the remaining challenges is clarifying a relationship between the crystal structure and the spin-related properties. It is well known that the atomic arrangement between ferromagnetic material and nonmagnetic material is a major factor of the spin polarization of injected electrons. Considering that the WF strongly depends on the atomic arrangement, the interfacial resistance of the ferromagnetic material–nonmagnetic material interface is also expected to be dependent on the atomic arrangement. Therefore, more efficient modulation of the interfacial resistance with a sizeable spin polarization might be possible by controlling the crystal structures of $Fe_{100-x}Gd_x$. Whereas growth techniques for epitaxial growth of $Fe_{100-x}Gd_x$ on Si with different crystal orientation have not been established so far, systematic research focusing on the atomic arrangement would be important for the innovation of next-generation spintronic devices.

ACKNOWLEDGMENTS

N.Y. acknowledges support from the Japan Society of the Promotion of Science (JSPS) Research Fellow Program (Grant No. 20J22776). A part of this study was supported by a Grant-in-Aid for Scientific Research from the Ministry of Education, Culture, Sports, Science and Technology (MEXT) of Japan, Grant-in-Aid for Scientific Research (S) "Semiconductor Spincurrentronics" No. 16H06330, Grant-in-Aid for Scientific Research (B) 19H02197 and 20H02607, Grant-in-Aid for Scientific Research (A) 22H00214, and Grant-in-Aid for Research Activity Start-up 20K22413, and by Japan Science and Technology Agency (JST), JST-PRESTO 'Information Carrier', Grant No. JPMJPR20B2, by Adaptable and Seamless Technology transfer Program through Target-driven R&D (A-STEP) Grant No. JPMJTR20RN, and by Kansai Research foundation for Technology Promotion. N.Y. also acknowledges the JSPS Research Fellowship (DC1), Tateishi Science and Technology Foundation (Grant No. C2207007), and the WISE Program "Innovation of Advanced Photonic and Electronic Devices" at Kyoto University. A part of this work was supported by the Kyoto University Nano Technology Hub in "Nanotechnology Platform Project" sponsored by MEXT, Japan. A part of this work was conducted in Nagoya Institute of Technology, supported by Advanced Research Infrastructure for Materials and Nanotechnology (JPMXP1222NI1501) of the Ministry of Education, Culture, Sports, Science and Technology (MEXT), Japan. The authors are grateful to Dr. Yasuyuki Kondo for his fruitful discussion on the physics of the drastic change in the work function and Dr. Mitsuaki Kaneko for his fruitful advice on the measurements of the Schottky barrier height.

N.Y. carried out the experiments and analyzed the data. S.H. carried out the first-principles calculation. N.Y., E.S., and Y.A. conceived the experiments. N.Y., M.S., and Y.A. wrote the manuscript. All the authors discussed the results.

[1] E. C. Stoner, Collective electron ferromagnetism II. Energy and specific heat, Proc. Math. Phys. Eng. Sci. **169**, 938 (1939).

[2] H. B. Michaelson, The work function of the elements and its periodicity, J. Appl. Phys. **48**, 4729 (1977).

[3] S. Gupta, F. Rortais, R. Ohshima, Y. Ando, T. Endo, Y. Miyata, and M. Shiraishi, Monolayer MoS_2 field effect transistor with low Schottky barrier height with ferromagnetic metal contacts, Sci. Rep. **9**, 17032 (2019).

[4] R. T. Tung, The physics and chemistry of the Schottky barrier height, Appl. Phys. Rev. **1**, 011304 (2014).

[5] R. J. Elliott, Theory of the effect of spin-orbit coupling on magnetic resonance in some semiconductors, Phys. Rev. **96**, 266 (1954).

[6] D. Basu, D. Saha, and P. Bhattacharya, Optical Polarization Modulation and Gain Anisotropy in An Electrically Injected Spin Laser, Phys. Rev. Lett. **102**, 093904 (2009).

[7] K. D. Yang, Y. Ha, U. Sim, J. An, C. W. Lee, K. Jin, Y. Kim, J. Park, J. S. Hong, J. H. Lee, H.- E. Lee, H.- Y. Jeong, H. Kim, and K. T. Nam, Graphene quantum sheet catalyzed silicon photocathode for selective CO_2 conversion to CO, Adv. Funct. Mater. **26**, 233 (2016).

[8] S. Sugahara and M. Tanaka, A spin metal-oxide-semiconductor field-effect transistor using half-metallic-ferromagnet contacts for the source and drain, Appl. Phys. Lett. **84**, 2307 (2004).

[9] H. Dery, P. Dalal, Cywiński, and L. J. Sham, Spin-based logic in semiconductors for reconfigurable large-scale circuits, Nature (London) **447**, 573 (2007).

[10] See Supplemental Material at http://link.aps.org/supplemental/10.1103/PhysRevMaterials.6.104405 for more detail on the crystal structure of thin films, procedures for analyzing the UV photoelectron spectroscopy spectra, first-principles calculation of bcc-Fe and hcp-Gd, the height of the Schottky barrier arising at the interface, repeatability of room-temperature ferrimagnetism, and calculation of magnetoresistance in Si-based spin devices with various interfacial resistance.

[11] M. Yoshitake, Principle and practical tips of work function measurement using UPS, XPS and AES instruments, Hyomen Kagaku **28**, 397 (2007).

[12] G. Kresse and J. Hafner, *Ab initio* molecular dynamics for liquid metals, Phys. Rev. B **47**, 558 (1993).

[13] G. Kresse and D. Joubert, From ultrasoft pseudopotentials to the projector augmented-wave method, Phys. Rev. B. **59**, 1758 (1999).

[14] J. P. Perdew, K. Burke, and M. Ernzerhof, Generalized Gradient Approximation Made Simple, Phys. Rev. Lett. **77**, 3865 (1996).

[15] K. R. Jeon, B. C. Min, Y. H. Jo, H. S. Lee, I. J. Shin, C. Y. Park, S. Y. Park, and S. C. Shin, Electrical spin injection and accumulation in CoFe/MgO/Ge contacts at room temperature, Phys. Rev. B **84**, 165315 (2011).

[16] S. Saito and T. Maeda, Work function of Fe-Ni alloy system, Vacuum **24**, 220 (1981).

[17] T. Soumiya, K. Ueda, N. Fukatani, T. Miyawaki, and H. Asano, Ferromagnetic Schottky junctions using diamond semiconductors, J. Magn. Soc. Japan **36**, 297 (2012).

[18] R. Bouwman and W. M. H. Sachtler, Photoelectric determination of gold-platinum of the work alloys function, J. Catal. **140**, 127 (1970).

[19] W. M. H. Sachter and G. J. H. Dorgelo, The surface of copper-nickel alloy films, J. Catal. **4**, 654 (1965).

[20] J. A. Rothschild, A. Cohen, A. Brusilovsky, L. Kornblum, Y. Kauffmann, Y. Amouyal, and M. Eizenberg, Fermi level tuning using the Hf-Ni alloy system as a gate electrode in metal-oxide-semiconductor devices, J. Appl. Phys. **112**, 013717 (2012).

[21] R. Bouwman, G. J. M. Lippits, and W. M. H. Sachtler, Photoelectric investigation of the surface composition of equilibrated AgGd alloys in ultrahigh vacuum and in the presence of CO, J. Catal. **25**, 350 (1972).

[22] S. C. Fain and J. M. McDavid, Work-function variation with alloy composition: Ag-Au, Phys. Rev. B **9**, 5099 (1974).

[23] J. Orehotsky and K. Scroder, Magnetic properties of amorphous Fe_x Gd_y alloy thin films, J. Appl. Phys. **43**, 2413 (1972).

[24] P. Mohn and E. P. Wohlfarth, The Curie temperature of the ferromagnetic transition metals and their compounds, J. Phys. F Met. Phys. **17**, 2421 (1987).

[25] V. Ambegaokar, B. I. Halperin, and J. S. Langer, Hopping conductivity in disordered systems, Phys. Rev. B **4**, 2612 (1971).

[26] N. Nagaosa, J. Sinova, S. Onoda, A. H. MacDonald, and N. P. Ong, Anomalous Hall effect, Rev. Mod. Phys. **82**, 1539 (2010).

[27] R. T. Tung, Schottky barrier height: Do we really understand what we measure?, J. Vac. Sci. Technol. B Microelectron. Nanom. Struct. **11**, 1546 (1993).

[28] S. M. Sze., *Semiconductor Devices: Physics and Technology*, 2nd ed. (Wiley, Hoboken, NJ, USA, 2002).

[29] B. L. Anderson and R. L. Anderson, *Fundamentals of Semiconductor Devices* (McGraw-Hill, New York, 2004).

[30] M. Schlüter, Chemical trends in metal-semiconductor barrier heights, Phys. Rev. B **17**, 5044 (1978).

[31] K. Murali, M. Dandu, K. Watanabe, T. Taniguchi, and K. Majumdar, Accurate extraction of Schottky barrier height and universality of Fermi level de-pinning of van der Waals contacts, Adv. Funct. Mater. **31**, 2010513 (2021).

[32] T. Sasaki, T. Oikawa, T. Suzuki, M. Shiraishi, Y. Suzuki, and K. Tagami, Electrical spin injection into silicon using MgO tunnel barrier, Appl. Phys. Express **2**, 053003 (2009).

[33] S. Sato, M. Tanaka, and R. Nakane, Spin transport in Si-based spin metal-oxide-semiconductor field-effect transistors: Spin drift effect in the inversion channel and spin relaxation in the n^+-Si source/drain regions, Phys. Rev. B **102**, 035305 (2020).

[34] S. Lee, F. Rortais, R. Ohshima, Y. Ando, S. Miwa, Y. Suzuki, H. Koike, and M. Shiraishi, Quantitative and systematic analysis of bias dependence of spin accumulation voltage in a nondegenerate Si-based spin valve, Phys. Rev. B **99**, 064408 (2019).

[35] E. I. Rashba, Theory of electrical spin injection: Tunnel contacts as a solution of the conductivity mismatch problem, Phys. Rev. B **62**, R16267 (2000).

[36] A. Fert and H. Jaffrès, Conditions for efficient spin injection from a ferromagnetic metal into a semiconductor, Phys. Rev. B **64**, 184420 (2001).

[37] N. Yamashita, S. Lee, R. Ohshima, E. Shigematsu, H. Koike, Y. Suzuki, S. Miwa, M. Goto, Y. Ando, and M. Shiraishi, Enhancement of spin signals by thermal annealing in silicon-based lateral spin valves, AIP Adv. **10**, 095021 (2020).

[38] W. Yang, J. Shang, J. Wang, X. Shen, B. Cao, N. Peimyoo, C. Zou, Y. Chen, Y. Wang, C. Cong, W. Huang, and T. Yu, Electrically tunable valley-light emitting diode (vLED) based on CVD-grown monolayer WS_2, Nano Lett. **16**, 1560 (2016).

[39] A. Chanda, J. E. Shoup, N. Schulz, D. A. Arena, and H. Srikanth, Tunable competing magnetic anisotropies and spin reconfigurations in ferrimagnetic $Fe_{100-x}Gd_x$ alloy films, Phys. Rev. B **104**, 094404 (2021).

[40] E. Jesenská, T. Ishibashi, L. Beran, M. Pavelka, J. Hamrle, R. Antoš, J. Zázvorka, and M. Veis, Optical and magneto-optical properties of $Gd_xFe_{(100-x)}$ thin films close to the compensation point, Sci. Rep. **9**, 16547 (2019).